APPLICATION OF THE FRACTAL GEOMETRY METHODS FOR ANALYSIS OF OXIDE LAYER

GWOŹDZIK Monika[1], KULESZA Sławomir[2], BRAMOWICZ Mirosław[3]

[1]Czestochowa University of Technology, Faculty of Production Engineering and Materials Technology, Institute of Materials Engineering, Czestochowa, Poland, EU
[2]University of Warmia and Mazury in Olsztyn, Faculty of Mathematics and Computer Science, Olsztyn, Poland, EU
[3]University of Warmia and Mazury in Olsztyn, Faculty of Technical Sciences, Olsztyn, Poland, EU

Abstract

The paper contains results of fractal analysis of oxide layers formed on steels used in the power industry. The studies were carried out on elements taken from three steel grades: 13CrMo4-5 (T = 470 °C, t = 190000 h), X10CrMoVNb9-1 (T = 535 °C, t = 75000 h), 10CrMo9-10 (T = 575 °C, t = 100000 h). The oxide layer was studied at the inner and outer surface of the tube wall. The obtained results of studies have shown that the fractal analysis results are affected by operational parameters and by the type of formed oxide layers.

Keywords: Oxide layers, fractal analysis, surface topography

1. INTRODUCTION

At present the huge development in research equipment has taken place, especially using in surface engineering, such as: SEM, XRD, AFM, TEM [1-24]. Studies on oxidised layers are now carried out more and more often, with the application of atomic forces microscopy. Atomic Force Microscopy helps to study the texture of a large variety of solid materials by sampling their surface heights z(x,y) followed by numerical derivation of statistical and fractal characteristics. This method demonstrated its applicability for studies of various structures, including: thin diamond films [25], Fe nanoparticles on foreign substrates [26], and even magnetic domains [27]. AFM images exhibit specific texture of the surface under study associated with a number of statistical and fractal characteristics that can be derived from the autocorrelation function R (**Figure 1A**) defined as follows:

$$R(m,n)=\frac{1}{(N-n)(N-m)}\sum_{k=1}^{N-n}\sum_{l=1}^{N-m}\left(z(k+m,y+l)\cdot z(k,l)\right) \tag{1}$$

where: N - is the number of scan steps along given scan axis, while m, n - integers describing the lag between given image and its copy.

Even though real surfaces are formed in random processes, they might be anisotropic to a certain degree. Surface lay of this type can be characterized using the surface anisotropy ratio S_{tr}, defined as the fraction of extreme decay lengths τ along which autocorrelation function falls down from 1.0 to 0.2 [28]:

$$0 < S_{tr} = \frac{\tau_{a1}}{\tau_{a2}}\Big|_{R=1\to 0,2} \le 1 \tag{2}$$

where: a1, and a2 - are the axes of the fastest and the slowest autocorrelation decay, respectively (**Figure 1A**). As a rule of thumb, Str higher than 0.5, corresponds to isotropic surface, while lower than 0.3 - highly anisotropic. Surfaces under study can be also characterized in view of their scaling behavior. To this end the autocorrelation function R need to be re-computed into structure function S according to the formula [29]:

$$S(m,n) = 2S_q^2\left(1 - R(m,n)\right) \tag{3}$$

where: S_q is the root-mean-square surface roughness. Scaling laws define whether and how geometrical objects exhibit self-similar properties similar to fractals. Thomas and Thomas [30] showed that the structure function averaged along an arbitrary direction could be fit with a power-law dependence in a form:

$$S(\tau) = K\tau^{2(2-D)} \tag{4}$$

where D - is the fractal dimension, and K - pseudo-topothesy. As a rule, fractal dimension D influences the relative, whereas pseudo-topothesy K the absolute amplitude of surface variations over the wavelengths. As shown in **Figure 1B**, with increasing scale length this power-law behavior steadily vanishes, and the structure function asymptotically reaches $2S_q^2$ value. A point, at which this dependence breaks down is referred to as the corner frequency τ_c.

Functional parameters can be derived from the Firestone-Abbott curve (**Figure 1C**) also known as the bearing curve. The curve appears after height samples are arranged in a descending order and plotted on the percent scale, where 100 % corresponds to the lowest sample in the series. DIN 4776 standard specifies several characteristics that can be useful in describing topographical complexity of the surface, including:

a) kernel roughness depth S_k - thickness of the core at the flattest part of the bearing curve where the largest increase in material exists;
b) reduced peak height S_{pk}, reduced valley depth S_{vk} - thickness of the bearing curve above/below the core profile, respectively;
c) upper bearing area M_{r1}, lower bearing area M_{r2} - intersection points of horizontal lines plotted from both ends of the flattest tangent of the bearing curve with that curve that delimit peaks and valleys from the core, respectively.

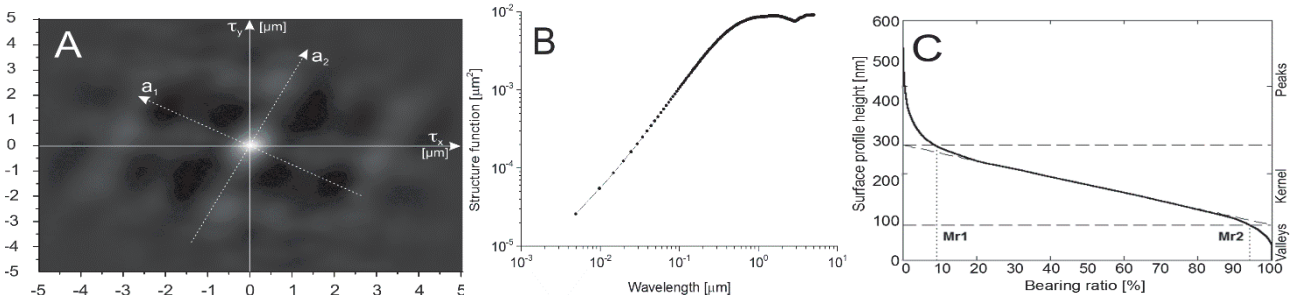

Figure 1 10CrMo9-10 steel - 3out: (A) Example plot of the autocorrelation function R with main directions of the anisotropy: a_1 and a_2. (B) Profile structure function vs. separation lag for monofractal structures. (C) Example Firestone-Abbott curve for determining functional properties of the surface under study

Table 1 Operating parameters of steel and designation of steel

Designation of steel			Operating parameters	
Steel	Kind of surface	Symbol	Temperature, °C	Time, h
13CrMo4-5	Inner	1in	470	190000
	Outer	1out		
X10CrMoVNb9-1	Inner	2in	535	70000
	Outer	2out		
10CrMo9-10	Inner	3in	575	100000
	Outer	3out		

2. MATERIALS AND EXPERIMENTAL METHODS

The material studied comprised specimens of 13CrMo4-5, X10CrMoVNb9-1 and 10CrMo9-10 steel taken from a pipeline operated for long time at an elevated temperature. The oxide layer was studied at the inner and outer surface of the tube wall. Operating parameters of steel and designation of steel were presented in **Table 1**. The topography measurements of oxide layer surface were studied using a Vecco atomic force microscope (AFM). The topography examinations were studied using Tapping Mode method. The study comprised a fractal analysis of oxide layers formed on steels long-term operated at elevated temperatures.

3. RESULTS OF EXAMINATION

Figure 2 presents AFM images of the studied samples surface. The coexistence of two structure types: large grains of irregular shape and sizes were approx. 2-3 μm and growing out from them clusters of smaller grains, not exceeding 500 nm, is a common feature of most of surface images. The coexistence of both structures causes a high variability of the surface height, which reaches 2 μm in the case of samples A-D in **Figure 2**. Samples 3in and 3out (images E and F in **Figure 2**) show a slightly different topography. In this case the surface is much flatter, because small grains exist on it and the presence of larger grains cannot be observed. This results in a smaller variability of the surface height, which in both cases does not exceed 1 μm. The obtained results S_{tr} show (**Table 2**) that the studied surfaces present a high variability of anisotropy, falling within the range from 0.33 (an anisotropic surface) to 0.99 (a perfectly isotropic surface). If in the case of 'in' samples it is possible to find a trend of growing isotropy (an increase from 0.33 to 0.78), then in the case of successive 'out' samples such trend was not found. Instead, it has turned out that the '1out' sample is perfectly isotropic, '2out' - anisotropic, while '3out' again highly isotropic. All the analysed layers have turned out to be mono-fractal structures (with the exception of '3in'), which means that in the entire studied length range the relative and absolute changes of the surface height can be described using only one index of the scale, i.e. a single value of fractal dimension D. The obtained D values fall within the range from 2.28 to 2.43, which proved a moderate development of the studied surfaces. However, it is difficult to find some clear relationship for values D between samples. This is strange inasmuch as that AFM images (**Figure 2**) suggest the coexistence of two structures of different characteristic dimensions, which should have converted into a bi-fractal characteristic of the surface. Only in the case of '3in' sample a clear bi-fractal nature of the surface was found, manifesting itself in substantially differing values of fractal dimension D for various ranges of the characteristic length. Taking into account the values of corner frequencyτ_c, hence the length of autocorrelation shift, for which the exponential scaling law transforms into a constant function, it is possible to notice a trend of decreasing values of this parameter while moving from samples 1, through 2, up to 3. It is also possible to add that if the series of 'out' samples shows a trend of a diminishing corner frequency (from 787 to 488 nm), then in the case of 'in' samples the changes are not monotonic. What is important, the exponential scaling law very quickly transforms into a constant function, because the length of shift does not exceed 15 per cent of the scanned area length. Core thickness S_k determines the working thickness of the surface layer, which is responsible for tribological properties ins a long period of operation. Small S_k values correspond to higher mechanical resistance and load capacity in applications, in which the studied surface is in direct contact with another surface. In the studied cases the value of S_k (**Table 3**) was basically decreasing, moving from the series 1 samples (500-1000 nm), via 2 (340-430 nm) to 3 (180-240 nm), which may be related to the reduction or even disappearance of large grains visible in **Figure 2**. The reduced peak height S_{pk} shows a similar decreasing trend, but only with respect to 'in' samples series, for which the value of S_{pk} was seen to fall from approx. 540 nm to 240 nm. In the case of 'out' samples series we would have observed a constant value of S_{pk} of around 570 nm, if it were not for sample 2out, for which the S_{pk} value goes up to 710 nm. As the S_{pk} defines the surface layer thickness, which quickly disappears in contact with another surface due to abrasion processes, the obtained values convert into the duration of the surface running-in process, if it is to transfer loads.

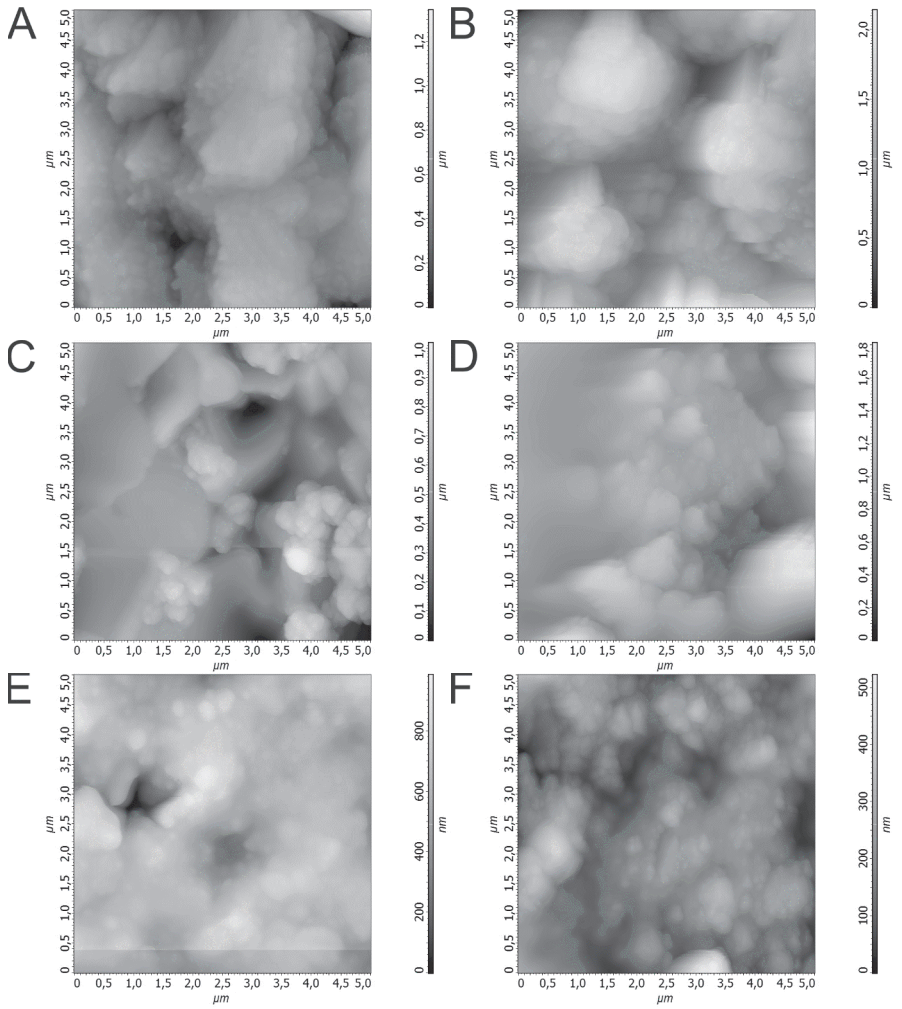

Figure 2 Surface topography of samples: (A) 1in, (B) 1out, (C) 2in, (D) 2out, (E) 3in, (F) 3out

Table 2 The statistical and fractal parameters: S_{tr} - the surface anisotropy ratio, D - the fractal dimension, τ_c - the corner frequency

Symbol of samples	S_{tr}	D_1	τ_{c1} [nm]	D_2	τ_{c2} [nm]		Symbol of samples	S_{tr}	D_1	τ_{c1} [nm]	D_2	τ_{c2} [nm]
1in	0.33			2.43	755		2out	0.36			2.39	630
1out	0.99			2.36	787		3in	0.78	2.52	32	2.35	554
2in	0.68			2.28	468		3out	0.61			2.32	488

Small values of S_{pk} are favourable from this point of view, with corresponding short running-in periods. In the discussed case the values of S_{pk} reach the same orders of magnitude as S_k. The upper bearing area M_{r1} is a similar parameter, describing a relative share of peaks in the total surface layer thickness. In the studied case M_{r1} ranges from 4.8 to 14.5 %, where lower values correspond to samples 1 and 3, while higher ones were found for samples of series 2. On the other hand, the depth of channels in the surface layer, in which the process fluids may be transported, is described by parameter S_{vk}, defining the thickness of layer remaining after the running-in process. From this point of view the obtaining of high S_{vk} values is favourable. The lower bearing index M_{r2} has a similar meaning; its complement to 100% defines the percentage share of channels in the total surface layer thickness. In the analysed cases the S_{vk} values were obtained within the range of 270 - 650 nm, except for sample 3out, for which S_{vk} was determined as around 80 nm.

Table 3 The functional parameters: S_k - kernel roughness depth, S_{pk} - reduced peak height, S_{vk} - reduced valley depth, M_{r1}/M_{r2} - upper/lower bearing area

Symbol of samples	S_k [nm]	S_{pk} [nm]	S_{vk} [nm]	M_{r1} [%]	M_{r2} [%]		Symbol of samples	S_k [nm]	S_{pk} [nm]	S_{vk} [nm]	M_{r1} [%]	M_{r2} [%]
1in	504.12	545.53	279.36	4.8	90.7		2out	436.4	711.31	654.29	14.5	88.3
1out	1017	572.73	545.88	12.8	96.1		3in	243.48	237.40	497.82	10.9	84.6
2in	341.53	404.30	272.16	11.3	88.1		3out	183.34	571.08	81.07	9.1	93.9

4. CONCLUSIONS

The fractal analysis was performed in the study on samples taken from three steel grades: two low-alloy steels (13CrMo4-5 and 10CrMo9-10), and 1 high-alloy steel (X10CrMoVNb9-1). The studies carried out both on the inside and on the outside have shown the coexistence of both large grains (2-3 μm) and much smaller ones, of approx. 500 nm size. Such structures were observed in all samples, except for the sample of 10CrMo9-10 steel, on which larger grains were visible. This is proven by the fact that for this steel at these operational parameters the previous studies have shown that on the inside the oxide layer is monolithic (only magnetite Fe_3O_4 exists). For samples taken from the inside of tube wall the isotropy was seen to grow with the increasing operating temperature. Instead, for samples taken from the outside such relationship was not found. The value of parameter S_{tr} for steels 13CrMo4-5 and 10CrMo9-10 shows that samples are isotropic, while the layer of oxides originated on the high-alloy steel - anisotropic. A similar relationship was observed for parameter S_{pk}, where for samples from the 'in' series this parameter goes down with increasing temperature. Instead, for the outside of the high-alloy steel (2out), contrary to oxides on low-alloy steel (1out and 3out), the value of coefficient S_{pk} is the highest. Additionally, the type of formed oxide layers affects the fractal parameters, where on the inside there are usually oxides built of one or a few layers, depending on the steel grade (Fe_2O_3, Fe_3O_4, Fe_3O_4+$FeCr_2O_4$), without deposits. On the outside the values of these parameters may be distorted by the additionally forming deposits.

REFERENCES

[1] GWOŹDZIK, M. Analysis of crystallite size changes in an oxide layer formed on steel used in the power industry. *Acta Physica Polonica A*, 2016, vol. 130, no. 4, pp. 935-938.

[2] BANKIEWICZ, D., ENESTAM, S., YRJAS, P., HUPA, M. Experimental studies of Zn and Pb induced high temperature corrosion of two commercial boiler steels. *Fuel Processing Technology*, 2013, vol. 105, pp. 89-97.

[3] NAKAI, M., NAGAI, K., MURATA, Y., MORINAGA, M. Improvement in steam oxidation resistance of Fe-10%Cr-0.08%C steel by suppressing. *Corrosion Science*, 2006, vol. 48, pp. 3869-3885.

[4] GWOŹDZIK, M. The defects of oxide layers formed on 10CrMo9-10 steel operated for 200000 hours at an elevated temperature. *Archives of Metallurgy and Materials*, 2016, vol. 61, no. 2B, pp. 987-992.

[5] LAVERDE, D., GOMEZ-ACEBO, T., CASTRO, F. Continuous and oxidation of T91 ferritic steel under steam. *Corrosion Science*, 2004, vol. 46, pp. 613-631.

[6] ISHITSUKA, T., INOUE, Y., OGAWA, H. Effect of silicon on the steam oxidation resistance of a 9%Cr heat resistant steel. *Oxidation of Metals*, 2004, vol. 61, no. 1-2, pp. 125-142.

[7] GWOŹDZIK, M. Characteristic of crystallite sizes and lattice deformations changes in the oxide layer formed on steel operated for a long time at an elevated temperature. *Solid State Phenomena*, 2013, vol. 203-204, pp. 204-207.

[8] YIN, K., QIU, S., TANG, R., ZHANG, Q., ZHANG, L. Corrosion behavior of ferritic/martensitic steel P92 in supercritical water. *The Journal of Supercritical Fluids*, 2009, vol. 50, pp. 235-239.

[9] SANCHEZ, L., HIERRO, M. P., PEREZ, F. J. Effect of chromium content on the oxidation behaviour of ferritic steels for applications in steam atmospheres at high temperatures. *Oxidation of Metals*, 2009, vol. 71, no. 3-4, pp. 173-186.

[10] PRISS, J., ROJACZ, H. KLEVTSOV, I., DEDOV, A., WINKELMANN, H., BADISCH, E. High temperature corrosion of boiler steels in hydrochloric atmosphere under oil shale ashes. *Corrosion Sciences*, 2014, vol. 82, pp. 36-44.

[11] SUNDARARAJAN, T., KURODA, S., ABE, F. Steam oxidation of 80Ni-20Cr high-velocity oxyfuel coatings on 9Cr-1Mo steel: diffusion-induced phase transformations in the substrate adjacent to the coating. *Metallurgical and Materials Transactions A*, 2005, vol. 36A, pp. 2165-2174.

[12] ROJACZ, H., BIRKELBACH, F., WIDDER, L., VARGA, M. Scale adhesion, scratch and fracture behaviour of different oxides formed on iron based alloys at 700°C. *Wear*, 2017, vol. 380-381, pp. 126-136.

[13] KONIECZNY, J., LABISZ, K., POLOK-RUBINIEC, M., WŁODARCZYK-FIGIEL, A. Influence of aluminium alloy anodizing and casting methods on structure and functional properties. *Archives of Metallurgy and Materials*, 2016, vol. 61, no. 3, pp. 991-995.

[14] BISCHOFF, J., MOTTA, A. T., EICHFELD, C., COMSTOCK, R. J., CAO, G., ALLEN, T. R. Corrosion of ferritic-martensitic steels in steam and supercritical water. *Journal of Nuclear Materials*, 2013, vol. 441, no. 1-3, pp. 604-611.

[15] CHEN, Y., SRIDHARAN, K., ALLEN, T. R., UKAI, S. Mictrostructural examination of oxide layers formed on an oxide dispersion strengthened ferritic steel exposed to supercritical water. *Journal of Nuclear Materials*, 2006, vol. 359, no. 1-2, pp. 50-58.

[16] SUN, W., TIEU, A. K., JIANG, Z., ZHU, H., LU, C. Oxide scales growth of low-carbon steel at high temperatures. *Journal of Materials Processing Technology*, 2004, vol. 155-156, no. SI, pp. 1300-1306.

[17] SZAFARSKA, M., IWASZKO, J. Laser remelting treatment of plasma-sprayed Cr_2O_3 oxide coatings. *Archives of Metallurgy and Materials*, 2012, vol. 57, no. 1, pp. 215-221.

[18] LABISZ, K. Microstructure and mechanical properties of high power diode laser (HPDL) treated cast aluminium alloys. *Mat.-wiss. U. Werkstofftech*, 2014, vol. 45, no. 4, pp. 314-324.

[19] WANG, S. Q., WEI, M. X., WANG, F., CUI, X. H., CHEN, K. M. Effect of morfology of oxide scale on oxidation wear in hot working die steels. *Materials Science and Engineering A*, 2009, vol. 505, pp. 20-26.

[20] HANSSON, A. N., PANTLEON, K., GRUMSEN, F. B., SOMERS, M. A. J. Microstructure evolution during steam oxidation of a Nb stabilized austenitic stainless steel. *Oxidation of Metals*, 2010, vol. 73, pp. 289-309.

[21] TALEKAR, A., CHANDRA, D., CHELLAPPA, R., DAEMEN, J., TAMURA,N., KUNZ, M. Oxidation kinetics of high strength low alloy steels at elevated temperatures. *Corrosion Science*, 2008, vol. 50, pp. 2804-2815.

[22] SRODA, S., BAXTER, D., ARPONEN, M. The influence of alloying elements on the corrosion behaviour of ferritic steels in simulated combustion atmospheres. *Materials and Corrosion*, 2005, vol. 56, no. 11, pp. 791795.

[23] LABISZ, K., TAŃSKI, T., KREMZER, M., JANICKI, D. Effect of laser alloying on heat-treated light alloys. *International Journal of Materials Research*, 2017, vol. 108, no. 2, pp. 126-132.

[24] FRANGINI, S., MASCI, A., McPHAIL, S. J., SOCCIO, T., ZAZA, F. Degradation behavior of a commercial 13Cr ferritic stainless steel (SS405) exposed to an ambient air atmosphere for IT-SOFC interconnect applications. *Materials Chemistry and Physics*, 2014, vol. 144, no. 3, pp. 491-497.

[25] KULSZA, S., BRAMOWICZ M. A comparative study of correlation methods for determination of fractal parameters in surface characterization. *Applied Surface Science*, 2014, vol. 293, pp. 196-201.

[26] TALU, S., BRAMOWICZ, M., KULSZA, S., SHAFIEKHANI, A., GHADERI, A., MASHAYEKHI, F., SOLAYMANI, S. Microstructure and tribological properties of FeNPs@ aC: H films by micromorphology analysis and fractal geometry. *Industrial & Engineering Chemistry Research*, 2015, vol. 54, no. 33, pp. 8212-8218.

[27] CZAJA, P., MAZIARZ, W., PRZEWOŹNIK, J., ŻYWCZAK, A., OZGA, P., BRAMOWICZ, M., KULESZA, S., DUTKIEWICZ, J. Surface topography, microstructure and magnetic domains in Al for Sn substituted metamagnetic Ni-Mn-Sn Heusler alloy ribbons. *Intermetallics*, 2014, vol. 55, pp. 1-8.

[28] DONG, W. P., SULLIVAN, P. J., STOUT, K. J. Comprehensive study of parameters for characterizing 3-dimensional surface topography IV: Parameters for characterizing spatial and hybrid properties. *Wear*, 1994, vol. 178, no. 1-2, pp. 45-60.

[29] SAYLES, R. S., THOMAS, T. R. Spatial representation of surface roughness by means of structure function-practical alternative to correlation. *Wear*, 1977, vol. 42, no. 2, pp. 263-276.

[30] THOMAS, A., THOMAS, T. R. Digital analysis of very small scale surface roughness. Journal of Wave-Material Interaction, 1988, vol. 3, pp. 341-350.